Mechanical Analysis of Thick-walled Filament Wound Composite Pipes under Pure Torsion Load

Mechanical analysis of thick-walled filament wound composite pipes under pure torsion load: safety zones and optimal design

Tianyu Wang[1], Marina Menshykova[1*], Oleksandr Menshykov[1], Igor A. Guz[2], Naomi K. Bokedal[1]

[1] School of Engineering, University of Aberdeen, AB24 3UE, Scotland, UK

[2] School of Engineering and Physical Sciences, Heriot Watt University, EH14 4AS, UK

t.wang.18@abdn.ac.uk (T. Wang), m.menshykova@abdn.ac.uk (M. Menshykova), o.menshykov@abdn.ac.uk (O. Menshykov), i.guz@hw.ac.uk (I.A. Guz), naomi.bokedal@gmail.com (N.K. Bokedal)

Keywords: Composite, thick-walled composite pipe, torsional behaviour, safety zone, numerical simulation, Finite Element Analysis.

Abstract

Thick-walled composite pipes made of fibre reinforced laminate are good candidates to replace traditional metal counterparts in fabricating such as drive shafts and drilling pipes. In this paper, the behaviour of thick-walled composite pipes subjected to torsion load is considered. The developed finite elements model and three-dimensional elasticity solution are presented to analyse the stress state of the pipe. The modified Tsai-Hill failure criterion is adapted for the stress analysis. The distribution of failure coefficients through the pipe thickness for different lay-ups is calculated. The parametric study is carried out to investigate the effects of fibre orientations, stacking sequences, layer thicknesses and the magnitudes of torsion on the pipe performance. The torsional response shows sensitivity to changes in winding angle. Although 45° reinforcement angle provides the highest torsional stiffness, the results indicate that it is not always the optimal solution due to the torsional strength. For multi-layered composite pipes, the optimum solution for the winding angle depends on the configurations and the stacking sequences. Finally, a new approach for pipe lay-up design to withstand the applied load is suggested, introducing 'safety zones', which represents reasonable fibre orientation to resist torsion load.

The authors declare that all data supporting the findings of this study are available within the article.

1 Introduction

Last several decades the increase in use of composite materials for different applications was very noticeable. The reason is high stiffness, good strength-to-weight ratio, and excellent corrosion resistance of these materials. Pipes are often made of metals or alloys, making them dense and susceptible to corrosion. This can be problematic in corrosive environments and in circumstances when the component weight is a limiting factor, such as offshore riser technology. Composite materials offer a solution to these problems. Composite materials have been applied in civil, automotive, aerospace, oil and gas, biomedical as well as offshore and subsea industries. However, the deficiency in performance data, regulatory requirements, complex design procedures, and also the knowledge of component repairs, limit the implementation of composites [1, 2].

Many researchers have presented the studies of mechanical behaviours of pipes or tubes made of composites under service conditions. High-performance filament wound composite pipes are used in sub-sea and high-pressure oil and gas transportation. Especially composite pipe under internal and external pressure, tension load and thermomechanical loading were considered in a number of publications. In paper [1] the detailed review on the application of fibre reinforced pipes in oil and gas industry was presented. A stress and failure analysis of thick-walled composite pipes under external pressure was also conducted. 3D elasticity solution was used to study the stress and strain states of composite pipe subjected to internal pressure [3]. The study of stresses and deformations of fibre reinforced composite pipe subjected to combined loads (internal pressure and thermomechanical load) was presented in [4]. The analysis of marine hose with reinforced layers subjected to internal pressure was conducted in [5], comparing FE model with the analytical results and found them to be in agreement. Thick-walled multi layered filament composite and hybrid cylinders were considered in [6]. In the paper, the deformation and stress analysis were conducted for axial load and internal and external pressure. Research on composite pipes with inner and outer liners subjected to combined thermomechanical load, external pressure and tension load were conducted in [7, 8]. The effects of liner thickness, the magnitude of thermal loading and stacking sequence on the failure of composite pipe were investigated by FEM. Numerical modelling of thermoplastic composite pipes subjected to combined bending and thermomechanical loading [9], and internal pressure and thermomechanical loading [10] was presented, and stress and failure analysis conducted.

Research on the mechanics of composite pipes under torsion was not systematic, which included investigation of the effects of stacking sequence, winding angle and thickness of the composite layers on the stress / strain state of the pipe. One of the reasons is that the researchers are usually assume that the axial force, the pressure and the bending load are the main factors affecting the mechanisms of failure of the pipe offshore or onshore. The other reason could be that torsional forces applied to composite pipe, is associated with failure caused by buckling [11]. This is reasonable for thin-walled pipe structures, but for thick-walled structures, this view is inappropriate. The morphologic failure of thick-walled composite pipe is characterised by matrix cracking [12, 13] and chipping [14], fibre fracture [15–17] and splitting [18], which occur prior to buckling.

In industry composite pipes can be used as high-performance automotive drive shafts [19], helicopter blade linkages [20] and composite drill pipes [21, 22] for oil extraction. Mutasher [19] conducted a study of the hybrid aluminium/composite drive shaft torsional properties. He found that the winding angle, stacking sequence and

number of the layer have a significant influence on the static torque capacity. However, those experimental samples were limited to two specific sets of winding angles and stacking sequences. The evaluation of the capacity of kenaf yarn composite hollow shaft with and without inner aluminium layer under torsion load was presented in [23].

Quaresimin [24] studied the fatigue behaviour of unidirectional composite pipes under torsion/tension load. The terms of specimen geometry, specimen manufacturing and local stress state were carefully discussed. Thermoplastic composite pipes subjected to torsion and thermomechanical load were considered in [25]. In the paper the results of stress and failure analysis were presented. The problem was solved analytically, and the obtained results were compared with the experimental ones. Simplified analytical model was developed to study the dependance of shear strain on applied torque and torsional angle [26].

Natsuki [27] proposed the analytical method in computing the stress and deformation with considering the effect of shear couplings. The results proved that torsional behaviour strongly depends on the stacking sequence and winding angle but no further analysis was carried out. Stress and failure analysis of fibre composite pipes under torsional load was considered in [28], where analytical and numerical results were compared. The stresses through the thickness of multi-layered filament wound pipe were presented in [29], where the problem was solved analytically for axial, pressure, and torque loadings. The obtained analytical results were verified by comparing with experimental and finite element analysis. Jonnalagadda [30] presented an analytical model to derive the stress state of the thin-walled composite pipe subjected to bending and torsion loading.

In the current paper, we present a comprehensive failure analysis of thick-walled multi-layered filament wound pipes subjected to pure torsion load. The Finite Element (FE) model is developed to carry out the stress and failure analysis of composite pipe subjected to pure torsion load. The model is validated by the comparison with the 3D elasticity solution. The effect of fibre orientation, stacking sequence, magnitude of loading and layer thickness on the structural performance is investigated. Furthermore, the reasonable winding angles which are evaluated by the introduction of ‘safety zones’ is discussed.

2 Problem statement

We consider a long fibre reinforced layered composite pipe. The pipe is modelled in the cylindrical coordinate system, where r, θ, and z represent radial, hoop and axial coordinates, respectively. The total thickness of N-layered composite pipe is h. The ϕ is denoted as the angle between principal fibre direction and structural longitude direction. The inner and outer radii are r_i and r_o, respectively. The details of the 3D composite pipe model are shown in Figure 1.

Let us consider the elastic state of composite pipe working under small strains. For an axisymmetric pipe subjected to axisymmetric loading ($\frac{\partial}{\partial\theta} = 0$), the stresses and strains are independent of the θ coordinate. The displacements of the pipe in cylindrical coordinates are expressed as [3]:

$$u_r = u_r(r), \tag{1}$$

$$u_\theta = u_\theta(r, z), \tag{2}$$

$$u_z = u_z(z), \tag{3}$$

where u_r and u_z are not dependant on the axial and radial directions, respectively. For the layer k, the simplified strain-displacement relations can be written as [1, 3, 31]:

$$\varepsilon_r^{(k)} = \frac{du_r^{(k)}}{dr}, \tag{4}$$

$$\varepsilon_\theta^{(k)} = \frac{u_r^{(k)}}{r}, \tag{5}$$

$$\varepsilon_z^{(k)} = \varepsilon_0, \tag{6}$$

$$\gamma_{zr}^{(k)} = 0, \tag{7}$$

$$\gamma_{\theta r}^{(k)} = 0, \tag{8}$$

$$\gamma_{z\theta}^{(k)} = \gamma_0 r, \tag{9}$$

where γ_0 is the pipe twist per unit length, and ε_0 represents the axial strain for all layers. Consequently, the simplified equilibrium equations for an axisymmetric pipe are presented as [3]:

$$\frac{d\sigma_r^{(k)}}{dr} + \frac{\sigma_r^{(k)} - \sigma_\theta^{(k)}}{r} = 0, \tag{10}$$

$$\frac{d\tau_{\theta r}^{(k)}}{dr} + \frac{2\tau_{\theta r}^{(k)}}{r} = 0, \tag{11}$$

$$\frac{d\tau_{zr}^{(k)}}{dr} + \frac{\tau_{zr}^{(k)}}{r} = 0. \tag{12}$$

Then, the interlaminate shear stresses can be obtained: $\tau_{\theta r}^{(k)} = \frac{U^{(k)}}{r^2}$ and $\tau_{zr}^{(k)} = \frac{W^{(k)}}{r}$, where U, W are unknown integration constants.

Here, we use subscript 1 to represent the principal fibre direction, where subscripts 2 and 3 correspond to transverse directions. The constitutive equation for stress-strain relations of monoclinic material in cylindrical coordinates for layer k is expressed as [31]:

$$\begin{Bmatrix} \sigma_z \\ \sigma_\theta \\ \sigma_r \\ \tau_{\theta r} \\ \tau_{zr} \\ \tau_{z\theta} \end{Bmatrix}^{(k)} = \begin{bmatrix} \overline{C}_{11} & \overline{C}_{12} & \overline{C}_{13} & 0 & 0 & \overline{C}_{16} \\ \overline{C}_{12} & \overline{C}_{22} & \overline{C}_{23} & 0 & 0 & \overline{C}_{26} \\ \overline{C}_{13} & \overline{C}_{23} & \overline{C}_{33} & 0 & 0 & \overline{C}_{36} \\ 0 & 0 & 0 & \overline{C}_{44} & \overline{C}_{45} & 0 \\ 0 & 0 & 0 & \overline{C}_{45} & \overline{C}_{55} & 0 \\ \overline{C}_{16} & \overline{C}_{26} & \overline{C}_{36} & 0 & 0 & \overline{C}_{66} \end{bmatrix}^{(k)} \begin{Bmatrix} \varepsilon_z \\ \varepsilon_\theta \\ \varepsilon_r \\ \gamma_{\theta r} \\ \gamma_{zr} \\ \gamma_{z\theta} \end{Bmatrix}^{(k)}. \tag{13}$$

The radial displacement $u_r^{(k)}$ of the composite pipe can be written in the following way [3]:

$$u_r^{(k)} = D^{(k)} r^{\beta(k)} + E^{(k)} r^{-\beta(k)} + \alpha_1^{(k)} \varepsilon_0 r + \alpha_2^{(k)} \gamma_0 r^2, \tag{14}$$

where $\beta^{(k)} = \left(\frac{\overline{C}_{22}^{(k)}}{\overline{C}_{33}^{(k)}} \right)^{\frac{1}{2}}$, $\alpha_1^{(k)} = \frac{\overline{C}_{12}^{(k)} - \overline{C}_{13}^{(k)}}{\overline{C}_{33}^{(k)} - \overline{C}_{22}^{(k)}}$, $\alpha_2^{(k)} = \frac{\overline{C}_{26}^{(k)} - 2\overline{C}_{36}^{(k)}}{4\overline{C}_{33}^{(k)} - \overline{C}_{22}^{(k)}}$, and $D^{(k)}$, $E^{(k)}$ are integration constants.

The expression for radial displacement is the solution of the differential equation, which is obtained by substituting the stress-strain relation equation (13) into the equilibrium equation (10) using the strain-displacement relations (4)–(9).

Then, the radial and hoop strains can be expressed by substituting the radial displacement (14) into the strain-displacement relations (4) and (5), where [31]:

$$\varepsilon_r^{(k)} = \beta(k)D^{(k)}r^{\beta(k)-1} - \beta(k)E^{(k)}r^{-\beta(k)-1} + \alpha_1^{(k)}\varepsilon_0 + 2\alpha_2^{(k)}\gamma_0 r, \tag{15}$$

$$\varepsilon_\theta^{(k)} = D^{(k)}r^{\beta(k)-1} - E^{(k)}r^{-\beta(k)-1} + \alpha_1^{(k)}\varepsilon_0 + \alpha_2^{(k)}\gamma_0 r. \tag{15}$$

Substituting the strains of the orthotropic layer k into the constitutive equation (13), the stresses in the cylindrical coordinate system are obtained as follows:

$$\sigma_r^{(k)} = \left(\overline{C}_{13}^{(k)} + \left(\overline{C}_{23}^{(k)} + \overline{C}_{33}^{(k)}\right)\alpha_1^{(k)}\right)\varepsilon_0 + \left(\overline{C}_{36}^{(k)} + \left(\overline{C}_{23}^{(k)} + 2\overline{C}_{33}^{(k)}\right)\alpha_2^{(k)}\right)\gamma_0 r + \left(\overline{C}_{23}^{(k)} + \beta(k)\overline{C}_{33}^{(k)}\right)D^{(k)}r^{\beta(k)-1} + \left(\overline{C}_{23}^{(k)} - \beta(k)\overline{C}_{33}^{(k)}\right)E^{(k)}r^{-\beta(k)-1}, \tag{16}$$

$$\sigma_\theta^{(k)} = \left(\overline{C}_{12}^{(k)} + \left(\overline{C}_{22}^{(k)} + \overline{C}_{23}^{(k)}\right)\alpha_1^{(k)}\right)\varepsilon_0 + \left(\overline{C}_{26}^{(k)} + \left(\overline{C}_{22}^{(k)} + 2\overline{C}_{23}^{(k)}\right)\alpha_2^{(k)}\right)\gamma_0 r + \left(\overline{C}_{22}^{(k)} + \beta(k)\overline{C}_{23}^{(k)}\right)D^{(k)}r^{\beta(k)-1} + \left(\overline{C}_{22}^{(k)} - \beta(k)\overline{C}_{23}^{(k)}\right)E^{(k)}r^{-\beta(k)-1}, \tag{17}$$

$$\sigma_z^{(k)} = \left(\overline{C}_{11}^{(k)} + \left(\overline{C}_{13}^{(k)} + \overline{C}_{12}^{(k)}\right)\alpha_1^{(k)}\right)\varepsilon_0 + \left(\overline{C}_{16}^{(k)} + \left(\overline{C}_{12}^{(k)} + 2\overline{C}_{13}^{(k)}\right)\alpha_2^{(k)}\right)\gamma_0 r + \left(\overline{C}_{12}^{(k)} + \beta(k)\overline{C}_{13}^{(k)}\right)D^{(k)}r^{\beta(k)-1} + \left(\overline{C}_{12}^{(k)} - \beta(k)\overline{C}_{13}^{(k)}\right)E^{(k)}r^{-\beta(k)-1}, \tag{18}$$

$$\tau_{z\theta}^{(k)} = \left(\overline{C}_{16}^{(k)} + \left(\overline{C}_{26}^{(k)} + \overline{C}_{36}^{(k)}\right)\alpha_1^{(k)}\right)\varepsilon_0 + \left(\overline{C}_{66}^{(k)} + \left(\overline{C}_{26}^{(k)} + 2\overline{C}_{36}^{(k)}\right)\alpha_2^{(k)}\right)\gamma_0 r + \left(\overline{C}_{26}^{(k)} + \beta(k)\overline{C}_{36}^{(k)}\right)D^{(k)}r^{\beta(k)-1} + \left(\overline{C}_{26}^{(k)} - \beta(k)\overline{C}_{36}^{(k)}\right)E^{(k)}r^{-\beta(k)-1}. \tag{19}$$

To calculate the stresses in the pipe, the unknown integration constants must be found. This is done by first defining the boundary conditions. The radial and interlaminate shear stresses at the inner (i) and outer (o) surfaces for the case of pure torsion load are expressed as [3]:

$$\sigma_r^{(1)}(r_i) = \sigma_r^{(N)}(r_o) = 0, \quad \tau_{\theta r}^{(1)}(r_i) = \tau_{zr}^{(1)}(r_i) = 0, \quad \tau_{\theta r}^{(N)}(r_o) = \tau_{zr}^{(N)}(r_o) = 0. \tag{20}$$

We assume that the interfaces are perfectly bonded, so the displacements are continuous layer to layer. Therefore, continuity conditions in the interfaces are expressed as [3]:

$$u_r^{(k)}(r_k) = u_r^{(k+1)}(r_k),\ u_\theta^{(k)}(r_k) = u_\theta^{(k+1)}(r_k),\ \sigma_r^{(k)}(r_k) = \sigma_r^{(k+1)}(r_k),$$

$$\tau_{zr}^{(k)}(r_k) = \tau_{zr}^{(k+1)}(r_k),\ \tau_{\theta r}^{(k)}(r_k) = \tau_{\theta r}^{(k+1)}(r_k). \tag{21}$$

Substituting the boundary conditions into the interlaminate shear stress equations, the integration constants U and W are both equal to 0.

The axial force is considered by integrating the axial stress over the cross-sectional area of the pipe [31]. To determine the torsion load the moment of shear stress $\tau_{z\theta}$ is integrated over the area of cross-section. Considering the applied torsion load, T, the boundary conditions are expressed as [1]:

$$2\pi \sum_{k=1}^{N} \int_{r_{k-1}}^{r_k} \tau_{z\theta}^{(k)}(r) r^2 dr = T. \tag{22}$$

Solving the system of equations (24), with the details provided in Appendix A, which consists of equations for boundary conditions, continuity conditions and torque, the $2 \times N + 2$ unknown constants ($D^{(k)}$, $E^{(k)}$, ε_0, γ_0) can be determined:

$$\begin{Bmatrix} \mathrm{D}^{(k)} \\ \vdots \\ \mathrm{E}^{(k)} \\ \vdots \\ \varepsilon_0 \\ \gamma_0 \end{Bmatrix} = [\Psi] \begin{Bmatrix} 0 \\ 0 \\ \vdots \\ 0 \\ 0 \\ \mathrm{Torsion} \end{Bmatrix}. \tag{23}$$

Once the values are obtained, the through-thickness distribution of stresses and strains can be computed.

To predict the failure of the composite pipe subjected to torsion load, the hoop, axial and shear stresses in the cylindrical coordinate system should be transformed into the principal directions, where the transformation matrix is defined as [1]:

$$\begin{bmatrix} \sigma_1 \\ \sigma_2 \\ \tau \end{bmatrix} = \begin{bmatrix} m^2 & n^2 & 2mn \\ n^2 & m^2 & -2mn \\ -mn & mn & m^2 - n^2 \end{bmatrix} \begin{bmatrix} \sigma_z \\ \sigma_\theta \\ \tau_{z\theta} \end{bmatrix}, \tag{24}$$

where $m = cos(\phi)$ and $n = cos(\phi)$.

The failure prediction is obtained by substituting the transformed stresses into the appropriate failure criteria. In this study, the modified Tsai-Hill failure criterion was applied, which includes both compressive and tensile strengths of the unidirectional lamina [32]:

$$FC = \frac{\sigma_1^2}{X_T^2} - \frac{\sigma_1 \sigma_2}{X_T^2} + \frac{\sigma_2^2}{Y_T^2} + \frac{\tau_{12}^2}{S^2}, (\sigma_2 > 0), \quad FC = \frac{\sigma_1^2}{X_C^2} - \frac{\sigma_1 \sigma_2}{X_C^2} + \frac{\sigma_2^2}{Y_C^2} + \frac{\tau_{12}^2}{(S - \mu_L \sigma_2)^2}, (\sigma_2 < 0), \tag{25}$$

where material constant μ_L characterizing in-plane shear strength is chosen as recommended by Kawai and Saito [32]. Normally, the structure will be damaged when the failure coefficient is higher or equal to one.

3 Numerical model and its validation

A thick-walled composite pipe is modelled in ABAQUS/CAE 2019 which can be used to predict the stresses under mechanical loadings. The thick-walled composite pipe cross-section is partitioned into several layers, where all interfaces are assumed to be perfectly bonded. Kinematic constraints are applied to the model, and torsional load is applied symmetrically to both ends of the pipe. The length-to-pipe diameter ratio is more than four for all considered cases, and the results are analysed in the middle cross section of the pipe. The model was

meshed using the C3D20R element (quadratic brick element, with reduced integration) which shows an excellent behaviour for curved structures and has the capability to avoid hourglass and shear locking phenomena.

Convergence analysis was carried out in order to establish a reasonable mesh. In composite pipes each lamina has its own characteristics, and the plies are relatively thin, so setting the mesh relying on empirical experience can cause distortion. Therefore, we optimised the mesh by adopting the number of elements along the thickness direction and adjusting the mesh size in the axial and circumferential directions.

Simulation was conducted for the composite pipe made of T300/5208 subjected to torsion load of 10kNm. The stacking sequence of the pipe is $[+45°/-45°]$, and the simulated length of the pipe is 200mm. We picked the outermost values in the middle region of the pipe as the reference points. Figure 2 shows the relationship between the set ratio (global element vs through-ply element) and the stresses. Initially, the appropriate global dimension is set to ten, and then decreases by two units in turn, and the through-ply elements are incremented by two along the thickness direction from one element to five elements per layer. It could be concluded that increasing the through-ply elements and decreasing the global mesh size has a positive effect on mesh convergence.

With a global mesh of four, the difference between the results of axial, hoop, and shear for through-ply elements of five and three are 0.0131%, 0.0093% and 0.0301%, respectively. Setting five elements and three elements along the thickness direction produces close results. Therefore, to prevent elemental distortion, satisfy the computational accuracy and reduce computational time, we decided to choose an elemental density of 4 (global element) /3 (through-ply element). The elemental density of 4/3 was deemed suitable.

The 3D elasticity solution (3D-ES) and developed FEM models have been validated by comparing with published results [31]. A two-layered composite pipe with fibre orientations $[+45°/-45°]$ was modelled in ABAQUS and MATLAB-based code. Radial, hoop, axial and shear stresses through the wall thickness distribution were computed. The results were normalized, so the horizontal coordinate is denoted as normalized value $(r - r_i)/h$. For vertical coordinate, the stresses are normalized by the average axial stress σ_0 and average laminate shear stress τ_0 [31]:

$$\sigma_0 = \frac{P_x}{\pi(r_o^2 - r_i^2)}, \tag{26}$$

$$\tau_0 = \frac{3T_x}{2\pi(r_o^3 - r_i^3)}. \tag{27}$$

We consider a thick-walled pipe, so the ratio between pipe diameter D and the wall thickness h must be $D/h \leq 20$ (or for each layer of the considered pipe is $r_i/h = 5$). The magnitude of torsion load is 10kNm. The results are obtained for carbon epoxy (T300/5208) material. The material properties are presented in Figure 3. It can be seen that the present analytical and FEM results (MATLAB and ABAQUS) agree with the published Herakovich results [31] for radial, hoop and axial stresses, with the exception of the shear stress. These small errors are due to the differences in their calculation methods. The FEA based on energy conservation method is more accurate in obtaining solutions where stresses are transferred between elements, the accuracy of which

depends on the mesh size and nodes. In contrast, in the 3D-ES calculation, the intralaminar shear strain is assumed to be 0 based on several assumptions. In fact, values of the intralaminar shear strain are exist, but are very small, and it could cause some results in the computation of stresses. As the maximum error value is only 3%, the results are deemed reliable.

Table 1. The properties of composite materials [1, 31, 33].

Properties	E_1 GPa	E_2 GPa	G_{12} GPa	ν_{12}	ν_{23}	X_t MPa	Y_t MPa	X_c MPa	Y_c MPa	S MPa
T300/LY5052	135	8	3.8	0.27	0.49	1860	76	1470	85	98
T300/5208	132	10.8	5.65	0.24	0.59	1513	43.4	--	--	86.87

4 Results and discussion

In this section, a summary of the simulation results is presented. To discuss the effects of parameters on the structural performance, a filament wound composite pipe composed of carbon/epoxy T300/LY5052 is considered. The total thickness of the four-layered composite pipe is h=6mm and the inner radius of the pipe, is r_i=30mm.

4.1 Effects of varying fibre orientation

The effects of fibre orientation on stresses and failure coefficients are investigated. We consider the pipe with uniform layer thicknesses of 1.5mm subjected to 10kNm torsion load. As the published articles are not very comprehensive in their study of the mechanical properties of pipes under torsion loading, author has chosen $55°$, the winding angle that is considered by most [34–38] to be better at resisting the internal pressure. The $[+\phi_1/-\phi_1/+\phi_2/-\phi_2]$ is the most common type of stacking sequence for balanced composite pipes in previous studies [3, 4, 6, 18] and is easy to be manufactured in industry. Therefore, we here set the inner two layers to a fixed winding angle and then vary the winding angle of the outer two layers to investigate the effects of varying winding angles on performance of the pipe. Hence, the configuration of the structure is $[+55°/-55°/+\phi°/-\phi°]$, fibre orientations, ϕ varies between 0°, 30°, 45°, 60°, and 90°.

The 3D elasticity solution and finite element model results perfectly coincide (see Figure 4). As we can see, the radial and hoop stresses of outer layers increase with the increased magnitude of the winding angle. The radial and hoop stresses of outer layers with $\phi = 45°$ are twice as high as for $\phi = 30°$ and 1.5 times lower than for $\phi = 60°$. However, for the axial stress, the increase in reinforcement angle results in a decrease in axial stress. For shear stress, a dramatic jump is observed between layers with fibre orientation of $55°$ and $0°$ or $90°$.

To predict the failure, the modified Tsai-Hill failure criterion is used in the study. After the axial, hoop and shear stresses were obtained, we employed the Eq. (24) to transform the stresses from cylindrical coordinate system to principal material direction. Subsequently, the transformed stresses were substituted into Eq. (25) and

finally, the failure coefficients were computed. The material constant μ_L is 0.7 [32]. Based on the results (Figure 5), the failure coefficient has no difference in value for composite pipes with winding angles of 0° and 90°, and the largest failure coefficient for $\phi = 90°$ is roughly four times higher than the largest failure coefficient for $\phi = 45°$. Although the distribution curves of the failure coefficients are close, with the exception of 0° and 90°, it can still be observed that 45° has the smallest value of the failure coefficient, meaning that of the five different winding angles 45° is able to resist greater torsion load.

4.2 Effects of increasing magnitude of loading

In the current subchapter we will investigate the effects of increasing magnitude of loading on the structural performances. In Figure 6 the failure coefficients for pipe with fibre orientations $[+55°/-55°/+60°/-60°]$ are presented. The torsion loads vary between 5-25kNm. The increase in torque causes a significant increase in the shear stress in the adjacent layers, and it results in the failure coefficients at the interface increase gradually with the growth of torsion load. Moreover, the higher the torsion load, the larger the failure coefficients. The composite pipe can withstand torsion load less than 20kNm. In addition, Figure 6 demonstrates that the failure usually happens at the interface between the pipe layers.

4.3 Effects of varying stacking sequence and layer thickness

The layout of A- and B-Type composite pipes is illustrated in Figure 7, and Figures 8–11 present the variations of modified Tsai-Hill failure coefficient depending on the stacking sequence and layer thickness.

The failure coefficient distribution of composite pipes with stacking sequence $[+55°/-\phi°/+\phi°/-55°]$ (Type-1) is shown in Figure 8. The angles which allow the composite tube with uniform layers thickness to withstand torsion load of 20kNm vary from 33° to 55°. If we increase the layer thickness of the layers with $\pm\phi°$ fibre orientation to 2mm, and decrease the thickness of the layers with $\pm 55°$ fibre orientation to 1mm (A-type), the range of allowable fibre orientations would be expanded, varying from 31° to 58°. However, if we increase the layer thickness of $\pm 55°$ layers to 2mm and decrease the thickness of $\pm\phi°$ layers to 1mm (B-type), the suitable winding angles would be 42° to 47°.

The failure coefficient distribution of composite pipe designed with middle $-55°$ and $+55°$ fibre layers and inner and outer layers of opposite fibre orientation is shown in Figure 9. It is noticed that comparing with Type-1 pipe, the suitable fibre orientations of the pipe with lay-up $[+\phi°/-55°/+55°/-\phi°]$ (Type-2) are slightly expanded and vary from 28° to 57°. Meanwhile, the suitable winding angles for Type-2 pipe with B-type layer thickness are expanded, which vary from around 29° to 62° under 20kNm torsion load. However, for the pipe with A-type layer thickness the allowable winding angles are only 27° to 48°.

Through the thickness distribution of failure criterion coefficient of composite pipe with stacking sequence $[+55°/-55°/+\phi°/-\phi°]$ (Type-3) is illustrated in Figure 10. The suitable winding angles for Type-3 pipe vary from 30° to 56°. The lowest failure criterion coefficient for pipe with uniform layer thickness is lower than the

lowest of A-type. If we turn over the stacking sequence, design the pipe with outer $\pm 55°$ fibre layers and inner layers of opposite fibre orientation from $0°$ to $90°$ (Type-4), the range of suitable winding angles would shrink, which vary from $35°$ to $55°$ (Figure 11). The failure coefficient of Type-4 pipes presents a smooth distribution in the inner $[+\phi/-\phi]$ layers, and the maximum failure coefficient is just 2.5 at $\phi = 90°$. We could notice that the lowest failure coefficient of pipe with B-type thickness is over one, and the pipe will not be able to withstand the 20kNm torsion load for all winding angles. For the pipe with uniform layer thickness, the winding angles which allow the pipe with A-type layer thickness to withstand 20kNm torsion load vary from $33°$ to $56°$.

In the investigated cases the lowest failure criterion coefficient is not always for $\phi = 45°$ although the torsion property of a single lamina is at its best stiffness [31]. Furthermore, the effect of thickness variation on the failure coefficient is determined by the winding angle. When the winding angle is close to or at $0°$ or $90°$, i.e. its torsional stiffness is low, the effect of the thickness variation on the overall failure coefficient of the structure is significant. When the winding angle corresponds to a higher torsional stiffness, for example close to or at $45°$, even an appropriate increase in the thickness of these composite layers will less increase the resistance of the structure to torque. A comparison of the four stacking sequences indicates that stacking sequence influences the distribution of the failure coefficients and determines the magnitude of the difference of the failure coefficient between the layers. It could be found that the Type-4 of pipes has that the maximum failure coefficient is the smallest and the distribution of its failure coefficient is smoothly along the thickness direction.

4.4 Introduction of safety zones for composite pipe design

Based on the results obtained in the previous sections, the authors propose a new method to obtain the appropriate winding angles.

A study is conducted to evaluate the suitable winding angles of the balanced composite pipes with different lay-ups subjected to 20kNm torsion load. For the analysis, pipe with the layers of equal thickness of 1.5mm is considered. Since the failure coefficients in each layer is either in gradually increasing or decreasing order, only the layer edges points are selected as reference points (Figure 12).

We clearly observe the safety zones in each of the reference points in Figure 13. The safety zones are zones on the plot, which show the angles with less than 1 failure coefficient for the considered pipe. The overlap of the safety zones for all reference points will result in safety zone for the considered lay-up (Figure 14).

The appropriate fibre angles (safety zones) for the pipes with different stacking sequences are shown in Figure 15 and Figure 16, where we can see how the shape of safety zone depends on the stacking sequence. The introduction of safety zones allows us to accelerate the process of multi-layered filament wound composite pipe design, showing suitable angles for the pipe of particular size and lay-up subjected to the chosen load.

5 Conclusions

In this study, the effect of winding angle, magnitude of loading, stacking sequence, and layer thickness on the failure and the stress states of thick-walled composite pipes subjected to pure torsion load was investigated using the developed Finite Element model and three-dimensional elasticity solution. The following important findings were made:

- The effects of changes in winding angle on the torsional behaviours of the structure are significant. When composite pipes are reinforced with fibres with reinforcement angles close to $0°$ or $90°$, the failure coefficient is much larger than reinforcement angles from $40°$ to $50°$ due to the poor torsional stiffness.
- Increasing torsion loadings can significantly contribute to an increase in the interlaminar shear stress and thus to an increase in failure coefficient at the layers' interfaces.
- Increasing in the thickness of the laminae with higher torsional stiffness can effectively improve the torsional capacity of the structure.
- Variations in the stacking sequence not only affect the smoothness of the distribution of the failure coefficient, but also the optimal solution to resist a given torsional load. Comparing the failure coefficients of $[\pm 55°/\pm 45°]$ and $[\pm 45°/\pm 55°]$, it is apparent that selecting a winding angle with a higher torsional stiffness for the outer layer will increase the torsional strength of the structure.

In addition, to find the suitable fibre angles for the multi-layered pipes under torsion load the safety zones were introduced. Safety zones show the allowable angles for the particular lay-up and load magnitude, providing a wider range of options in design, making the design process of the filament wound pipe quicker.

6 References

[1] Guz, I.A., Menshykova, M. and Paik, J.K., (2017). Thick-walled composite tubes for offshore applications: an example of stress and failure analysis for filament-wound multi-layered pipes, *Ships and Offshore Structures*, **12** (3), pp.304-322.

[2] Cox, K., Menshykova, M., Menshykov, O. and Guz, I., (2019). Analysis of flexible composites for coiled tubing applications, *Composite Structures*, pp.111118.

[3] Xia, M., Takayanagi, H. and Kemmochi, K., (2001). Analysis of multi-layered filament-wound composite pipes under internal pressure, *Composite Structures*, **53** (4), pp.483-491.

[4] Bakaiyan, H., Hosseini, H. and Ameri, E., (2009). Analysis of multi-layered filament-wound composite pipes under combined internal pressure and thermomechanical loading with thermal variations, *Composite Structures*, **88** (4), pp.532-541.

[5] Zhou, Y., Duan, M., Ma, J. and Sun, G., (2018). Theoretical analysis of reinforcement layers in bonded flexible marine hose under internal pressure, *Engineering Structures*, **168** pp.384-398.

[6] Xing, J., Geng, P. and Yang, T., (2015). Stress and deformation of multiple winding angle hybrid filament-wound thick cylinder under axial loading and internal and external pressure, *Composite Structures,* **131** pp.868-877.

[7] Hastie, J.C., Guz, I.A. and Kashtalyan, M., (2019). Effects of thermal gradient on failure of a thermoplastic composite pipe (TCP) riser leg, *International Journal of Pressure Vessels and Piping,* **172** pp.90-99.

[8] Hastie, J.C., Kashtalyan, M. and Guz, I.A., (2019). Failure analysis of thermoplastic composite pipe (TCP) under combined pressure, tension and thermal gradient for an offshore riser application, *International Journal of Pressure Vessels and Piping,* **178** pp.103998.

[9] Hastie, J.C., Guz, I.A. and Kashtalyan, M., (2021). Numerical modelling of spoolable thermoplastic composite pipe (TCP) under combined bending and thermal load, *Ships and Offshore Structures,* pp.1-12.

[10] Hastie, J.C., Kashtalyan, M. and Guz, I.A., (2021). Analysis of filament-wound sandwich pipe under combined internal pressure and thermal load considering restrained and closed ends, *International Journal of Pressure Vessels and Piping,* pp.104350.

[11] Wicks, N., Wardle, B.L. and Pafitis, D., (2008). Horizontal cylinder-in-cylinder buckling under compression and torsion: Review and application to composite drill pipe, *International Journal of Mechanical Sciences,* **50** (3), pp.538-549.

[12] Sebaey, T.A., (2019). Design of oil and gas composite pipes for energy production, *Energy Procedia,* **162** pp.146-155.

[13] Maziz, A., Rechak, S. and Tarfaoui, M., (2021). Comparative study of tubular composite structure subjected to internal pressure loading: Analytical and numerical investigation, *Journal of Composite Materials,* **55** (11), pp.1517-1533.

[14] Gu, Y., Zhou, H., Zhang, D., Liu, J. and Wang, S., (2022). Torsional mechanical properties and failure mechanism of braided carbon fiber reinforced composite tubes, *Fangzhi Xuebao/Journal of Textile Research,* **43** (3), pp.95-102.

[15] Martins, L., Bastian, F. and Netto, T., (2013). The effect of stress ratio on the fracture morphology of filament wound composite tubes, *Materials & Design,* **49,** pp.471-484.

[16] Bisagni, C., (2009). Experimental investigation of the collapse modes and energy absorption characteristics of composite tubes, *International Journal of Crashworthiness,* **14** (4), pp.365-378.

[17] Özbek, Ö, Doğan, N.F. and Bozkurt, ÖY., (2020). An experimental investigation on lateral crushing response of glass/carbon intraply hybrid filament wound composite pipes, *Journal of the Brazilian Society of Mechanical Sciences and Engineering,* **42**(7), pp.1-13.

[18] Gemi, L., Köroğlu, M.A. and Ashour, A., (2018). Experimental study on compressive behavior and failure analysis of composite concrete confined by glass/epoxy ±55° filament wound pipes, *Composite Structures,* **187,** pp.157-168.

[19] Mutasher, S., (2009). Prediction of the torsional strength of the hybrid aluminum/composite drive shaft, *Materials & Design,* **30** (2), pp.215-220.

[20] Rasuo, B., (2018). 3.11 on structural damping of composite aircraft structures, In Beaumont, P.W.R. and Zweben, C.H., (Eds.) *Comprehensive Composite Materials II.* Oxford: Elsevier, pp. 288-299.

[21] Enamul Hossain, M., (2011). The current and future trends of composite materials: an experimental study, *Journal of Composite Materials,* **45** (20), pp.2133-2144.

[22] Leslie, J.C., Williamson, S., Long, R., Jean, J., Truong, L. and Nuebert, H., (2002). Composite drill pipe for extended-reach and deep water applications, *Offshore Technology Conference.*

[23] Misri, S., Sapuan, S., Leman, Z. and Ishak, M., (2015). Torsional behaviour of filament wound kenaf yarn fibre reinforced unsaturated polyester composite hollow shafts, *Materials & Design (1980-2015),* **65,** pp.953-960.

[24] Quaresimin, M. and Carraro, P., (2014). Damage initiation and evolution in glass/epoxy tubes subjected to combined tension–torsion fatigue loading, *International Journal of Fatigue,* **63,** pp.25-35.

[25] He, Y., Vaz, M.A. and Caire, M., (2021). Stress and failure analyses of thermoplastic composite pipes subjected to torsion and thermomechanical loading, *Marine Structures,* **79**, pp. 103024.

[26] Zhao, Y. and Pang, S., (1995). Stress-strain and failure analyses of composite pipe under torsion.

[27] Natsuki, T., Tsuda, H. and Kemmochi, K., (2003). Structural Analysis of Thick-Walled Filament-Wound Pipes. *Journal of the Society of Materials Science, Japan,* **52** (6), pp.606-611.

[28] Wang, T., Menshykov, O., Menshykova, M. and Guz, I., (2020). Modelling and optimal design of thick-walled composite pipes under in-service conditions, *IOP Conference Series: Materials Science and Engineering,* pp. 012046.

[29] Wang, T., Menshykova, M., Menshykov, O. and Guz, I., (2021). *Failure analysis of multi-layered thick-walled composite pipes subjected to torsion loading, Materials Science Forum,* **1047,** pp.25-30.

[30] Jonnalagadda, A., Sawant, A., Rohde, S., Sankar, B. and Ifju, P., (2015). An analytical model for composite tubes with bend–twist coupling, *Composite Structures,* **131,** pp.578-584.

[31] Herakovich, C.T., (1998). Mechanics of fibrous composites.

[32] Kawai, M. and Saito, S., (2009). *Off-axis strength differential effects in unidirectional carbon/epoxy laminates at different strain rates and predictions of associated failure envelopes, Composites Part A: Applied Science and Manufacturing,* **40**(10), pp.1632-1649.

[33] Cagdas, I.U., (2017). Optimal design of variable stiffness laminated composite truncated cones under lateral external pressure, *Ocean Engineering,* **145,** pp.268-276.

[34] Xia, M., Kemmochi, K. and Takayanagi, H., (2001). Analysis of filament-wound fiber-reinforced sandwich pipe under combined internal pressure and thermomechanical loading, *Composite Structures,* **51**(3), pp.273-283.

[35] Arikan, H., (2010). Failure analysis of $(\pm 55)_3$ filament wound composite pipes with an inclined surface crack under static internal pressure, *Composite Structures,* **92** (1), pp.182-187.

[36] Tarakçioğlu, N., Gemi, L. and Yapici, A., (2005). Fatigue failure behavior of glass/epoxy ±55 filament wound pipes under internal pressure, *Composites Science and Technology,* **65** (3-4), pp.703-708.

[37] Betts, D., Sadeghian, P. and Fam, A., (2019). Investigation of the stress-strain constitutive behavior of±55° filament wound GFRP pipes in compression and tension, *Composites Part B: Engineering,* **172,** pp.243-252.

[38] Tarakcioglu, N., Samanci, A., Arikan, H. and Akdemir, A., (2007). The fatigue behavior of $(\pm 55)_3$ filament wound GRP pipes with a surface crack under internal pressure, *Composite Structures,* **80** (2), pp.207-211.

Appendix A

$$\Psi(1,1) = \left(\overline{C}_{23}^{(1)} + \beta(1) \times \overline{C}_{33}^{(1)}\right) \times r_1^{\beta(1)-1}$$

$$\Psi(1, N+1) = \left(\overline{C}_{23}^{(1)} - \beta(1) \times \overline{C}_{33}^{(1)}\right) \times r_1^{-\beta(1)-1}$$

$$\Psi(1,2 \times N+1) = \overline{C}_{13}^{(1)} + \alpha_1^{(1)} \times \left(\overline{C}_{23}^{(1)} + \overline{C}_{33}^{(1)}\right)$$

$$\Psi(1,2 \times N+2) = \left(\overline{C}_{36}^{(1)} + \alpha_2^{(1)} \times \left(\overline{C}_{23}^{(1)} + 2 \times \overline{C}_{33}^{(1)}\right)\right) * r_1$$

$$\Psi(N+1,1) = \left(\overline{C}_{23}^{(1)} + \beta(1) \times \overline{C}_{33}^{(1)}\right) \times r_2^{\beta(1)-1}$$

$$\Psi(N+1,2) = -\left(\overline{C}_{23}^{(2)} + \beta(2) \times \overline{C}_{33}^{(2)}\right) \times r_2^{\beta(2)-1}$$

$$\Psi(N+1, N+1) = \left(\overline{C}_{23}^{(1)} - \beta(1) \times \overline{C}_{33}^{(1)}\right) \times r_2^{-\beta(1)-1}$$

$$\Psi(N+1, N+2) = -\left(\overline{C}_{23}^{(2)} + \beta(2) \times \overline{C}_{33}^{(2)}\right) \times r_2^{-\beta(2)-1}$$

$$\Psi(N+1,2 \times N+1) = \overline{C}_{13}^{(1)} - \overline{C}_{13}^{(2)} + \alpha_1^{(1)} \times \left(\overline{C}_{23}^{(1)} + \overline{C}_{33}^{(1)}\right) - \alpha_1^{(2)} \times \left(\overline{C}_{23}^{(2)} + \overline{C}_{33}^{(2)}\right)$$

$$\Psi(N+1,2 \times N+2) = \left(\overline{C}_{36}^{(1)} - \overline{C}_{36}^{(2)} + \alpha_2^{(1)} \times \left(\overline{C}_{23}^{(1)} + 2 \times \overline{C}_{33}^{(1)}\right) - \alpha_2^{(2)} \times \left(\overline{C}_{23}^{(2)} + 2 \times \overline{C}_{33}^{(2)}\right)\right) \times r_2$$

$$\Psi(2 \times N, N) = \left(\overline{C}_{23}^{(N)} + \beta(N) \times \overline{C}_{33}^{(N)}\right) \times r_{N+1}^{\beta(N)-1}$$

$$\Psi(2 \times N, 2 \times N) = \left(\overline{C}_{23}^{(N)} - \beta(N) \times \overline{C}_{33}^{(N)}\right) \times r_{N+1}^{-\beta(N)-1}$$

$$\Psi(2 \times N, 2 \times N+1) = \overline{C}_{13}^{(N)} + \alpha_1^{(N)} \times \left(\overline{C}_{23}^{(N)} + \overline{C}_{33}^{(N)}\right)$$

$$\Psi(2 \times N, 2 \times N+2) = \left(\overline{C}_{36}^{(N)} + \alpha_2^{(N)} \times \left(\overline{C}_{23}^{(N)} + 2 \times \overline{C}_{33}^{(N)}\right)\right) * r_{N+1}$$

$$\Psi(k, k-1) = r_k^{\beta(k-1)}$$

$$\Psi(k, k) = -r_k^{\beta(k)}$$

$$\Psi(k, k+N-1) = r_k^{-\beta(k-1)}$$

$$\Psi(k, k+N) = -r_k^{-\beta(k)}$$

$$\Psi(k, 2 \times N+1) = \left(\alpha_1^{(k-1)} - \alpha_1^{(k)}\right) \times r_k$$

$$\Psi(k, 2 \times N+2) = \left(\alpha_2^{(k-1)} - \alpha_2^{(k)}\right) \times r_k^2$$

$$\Psi(N+k-1, k-1) = \left(\overline{C}_{23}^{(k-1)} + \beta(k-1) \times \overline{C}_{33}^{(k-1)}\right) \times r_k^{\beta(k-1)-1}$$

$$\Psi(N+k-1, k) = -\left(\overline{C}_{23}^{(k)} + \beta(k) \times \overline{C}_{33}^{(k)}\right) \times r_k^{\beta(N)-1}$$

$$\Psi(N+k-1, N+k-1) = \left(\overline{C}_{23}^{(k-1)} - \beta(k-1) \times \overline{C}_{33}^{(k-1)}\right) \times r_k^{-\beta(k-1)-1}$$

$$\Psi(N+k-1, N+k) = -\left(\overline{C}_{23}^{(k)} - \beta(k) \times \overline{C}_{33}^{(k)}\right) \times r_k^{-\beta(N)-1}$$

$$\Psi(N+k-1,2 \times N+1) = \overline{C}_{13}^{(k-1)} - \overline{C}_{13}^{(k)} + \alpha_1^{(k-1)} \times \left(\overline{C}_{23}^{(k-1)} + \overline{C}_{33}^{(k-1)}\right) - \alpha_1^{(k)} \times \left(\overline{C}_{23}^{(k)} + \overline{C}_{33}^{(k)}\right)$$

$$\Psi(N+k-1,2 \times N+2)$$
$$= \left(\alpha_2^{(k-1)} \times \left(\overline{C}_{23}^{(k-1)} + 2 \times \overline{C}_{33}^{(k-1)}\right) - \alpha_2^{(k)} \times \left(\overline{C}_{23}^{(k)} + 2 \times \overline{C}_{33}^{(k)}\right) + \overline{C}_{36}^{(k-1)} - \overline{C}_{36}^{(k)}\right) * r_k$$

$$(k = 2 \ldots N)$$

$$\Psi(2 \times N+1, k) = \frac{\overline{C}_{12}^{(k)} + \beta(k) \times \overline{C}_{13}^{(k)}}{1+\beta(k)} \times \left(r_{k+1}^{\beta(k)+1} - r_k^{\beta(k)+1}\right)$$

$$\Psi(2\times N+1,N+k)=\frac{\overline{C}_{12}^{(k)}-\beta(k)\times\overline{C}_{13}^{(k)}}{1-\beta(k)}\times\left(r_{k+1}^{-\beta(k)+1}-r_{k}^{-\beta(k)+1}\right)$$

$$\Psi(2\times N+2,k)=\frac{\overline{C}_{26}^{(k)}+\beta(k)\times\overline{C}_{36}^{(k)}}{2+\beta(k)}\times\left(r_{k+1}^{\beta(k)+2}-r_{k}^{\beta(k)+2}\right)$$

$$\Psi(2\times N+2,N+k)=\frac{\overline{C}_{26}^{(k)}-\beta(k)\times\overline{C}_{36}^{(k)}}{2-\beta(k)}\times\left(r_{k+1}^{-\beta(k)+2}-r_{k}^{-\beta(k)+2}\right)$$

$$(k=1\dots N)$$

$$\Psi(2\times N+1,2\times N+1)=\sum_{1}^{N}\left(\overline{C}_{11}^{(k)}+\alpha_{1}^{(k)}\times\left(\overline{C}_{12}^{(k)}+\overline{C}_{13}^{(k)}\right)\right)\times\frac{r_{k+1}^{2}-r_{k}^{2}}{2}$$

$$\Psi(2\times N+1,2\times N+2)=\sum_{1}^{N}\left(\overline{C}_{16}^{(k)}+\alpha_{2}^{(k)}\times\left(\overline{C}_{12}^{(k)}+2\times\overline{C}_{13}^{(k)}\right)\right)\times\frac{r_{k+1}^{3}-r_{k}^{3}}{3}$$

$$\Psi(2\times N+2,2\times N+1)=\sum_{1}^{N}\left(\overline{C}_{16}^{(k)}+\alpha_{1}^{(k)}\times\left(\overline{C}_{26}^{(k)}+\overline{C}_{36}^{(k)}\right)\right)\times\frac{r_{k+1}^{3}-r_{k}^{3}}{3}$$

$$\Psi(2\times N+2,2\times N+2)=\sum_{1}^{N}\left(\overline{C}_{66}^{(k)}+\alpha_{2}^{(k)}\times\left(\overline{C}_{26}^{(k)}+2\times\overline{C}_{36}^{(k)}\right)\right)\times\frac{r_{k+1}^{4}-r_{k}^{4}}{4}$$

$$(k=1\dots N)$$

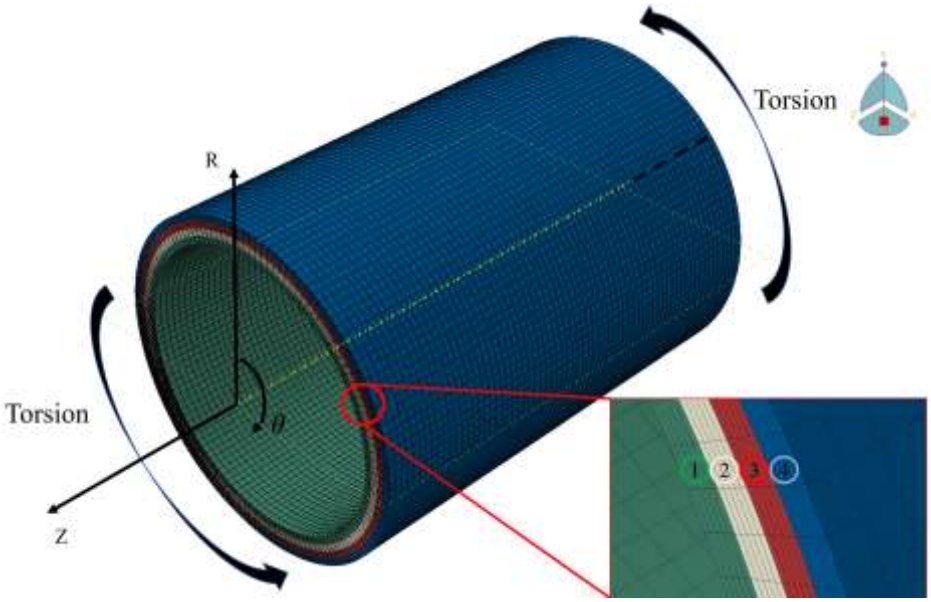

Figure 1. The three-dimensional composite pipe model in cylindrical coordinate system.

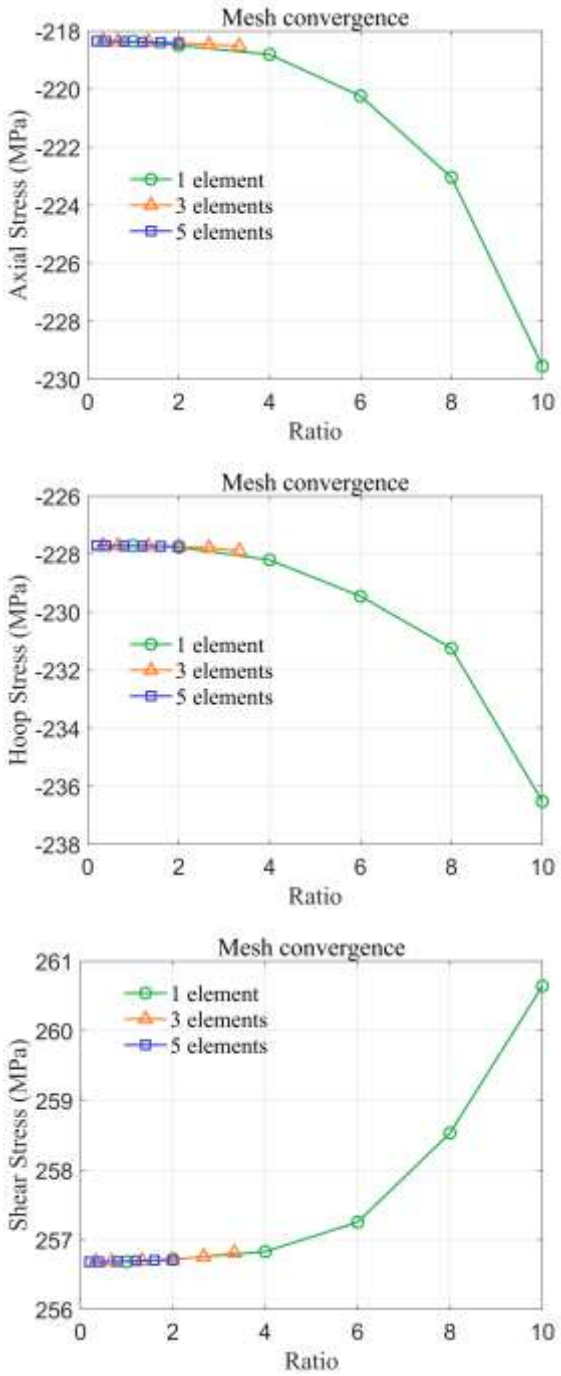

Figure 2. Dependence of the solution on the FE mesh.

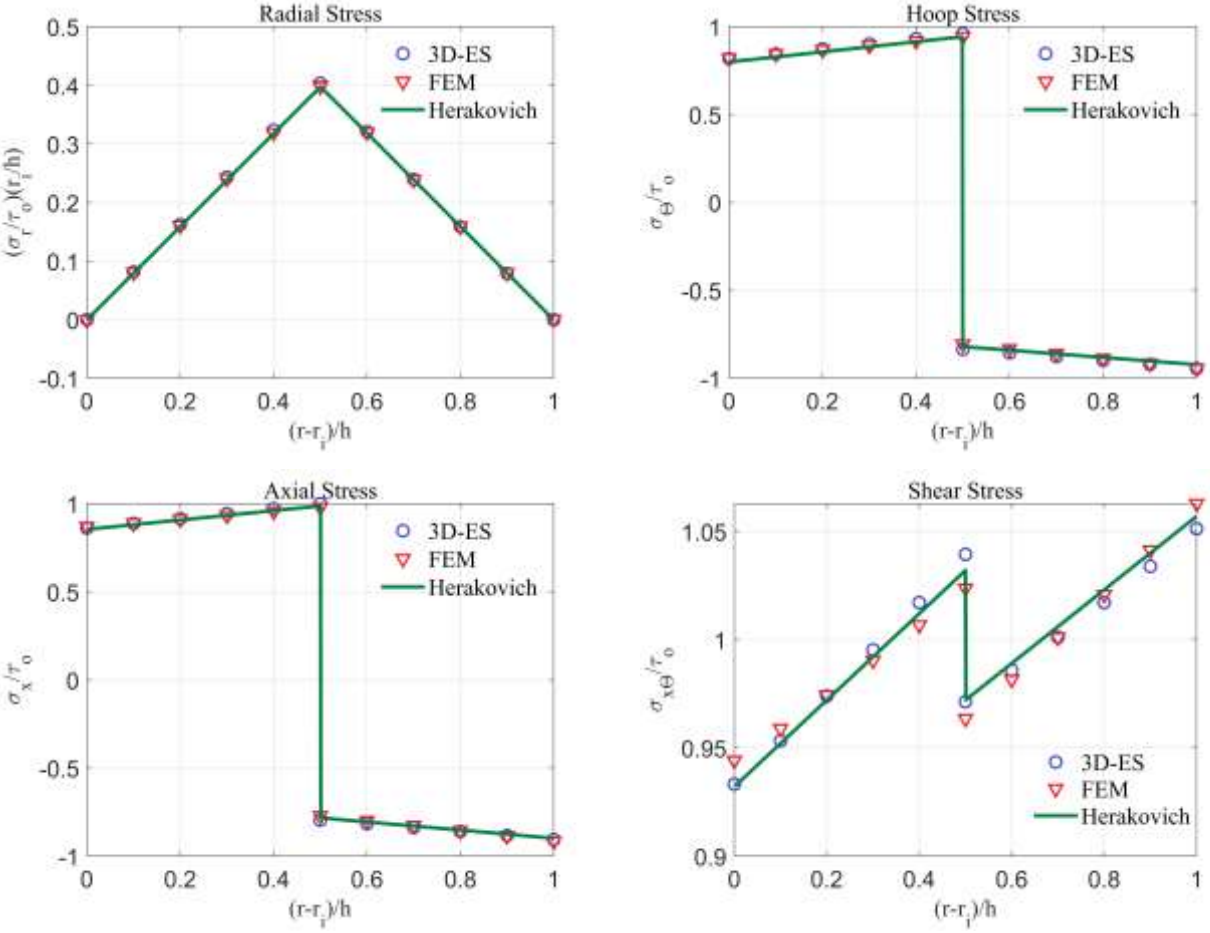

Figure 3. Comparison of analytical and FE models – normalized stresses across the normalized pipe thickness.

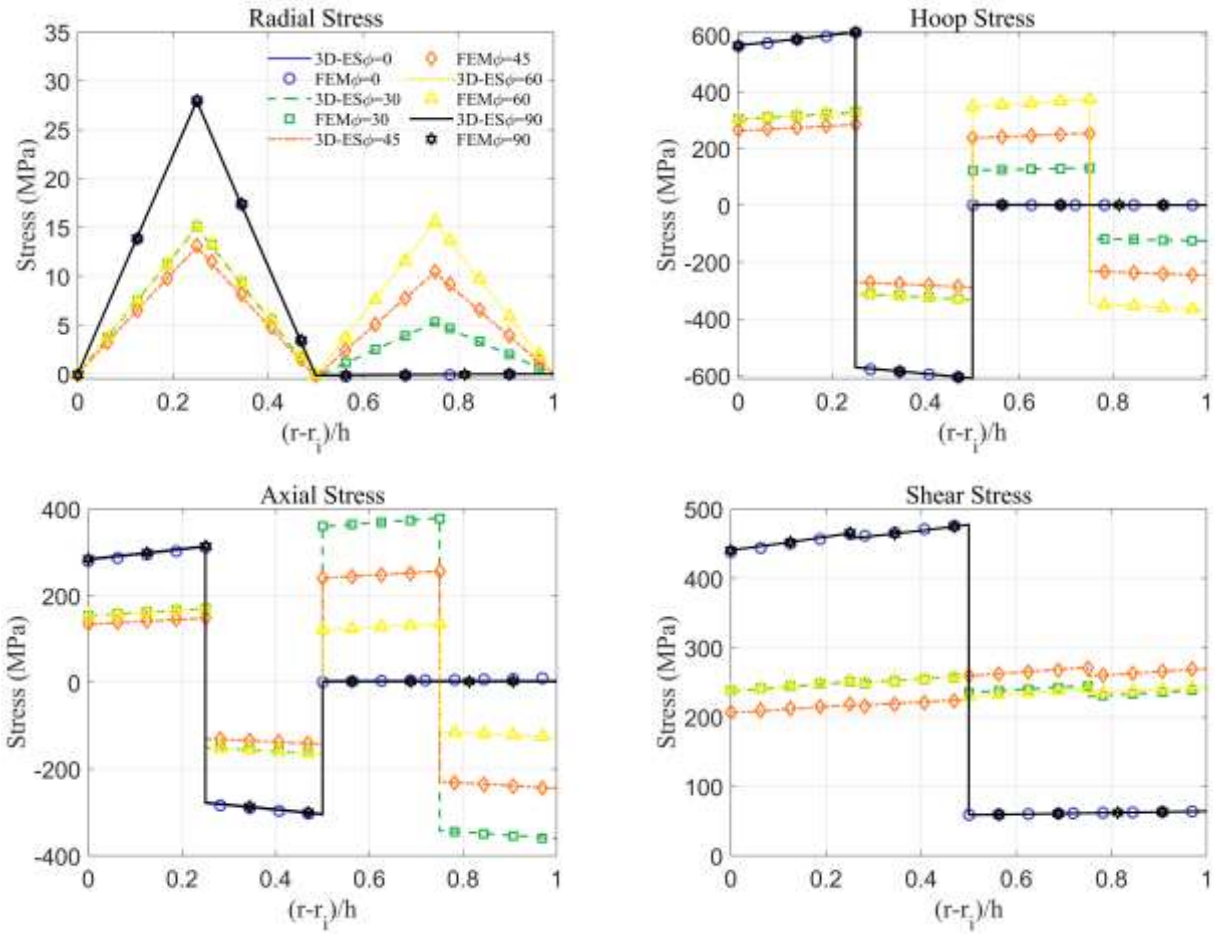

Figure 4. The radial, hoop, axial and shear stresses for different filament winding angles.

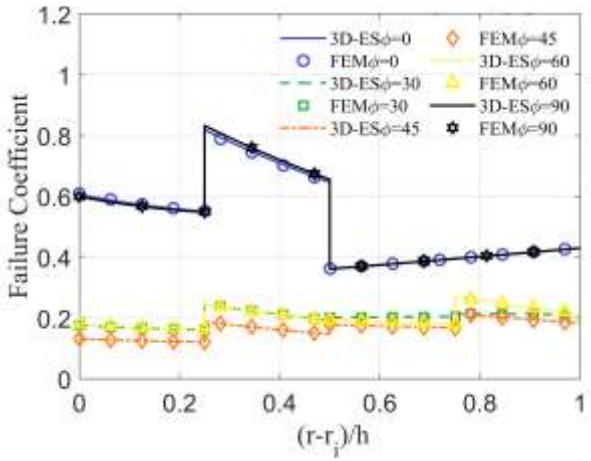

Figure 5. Modified Tsai-Hill failure coefficients across the normalized pipe thickness.

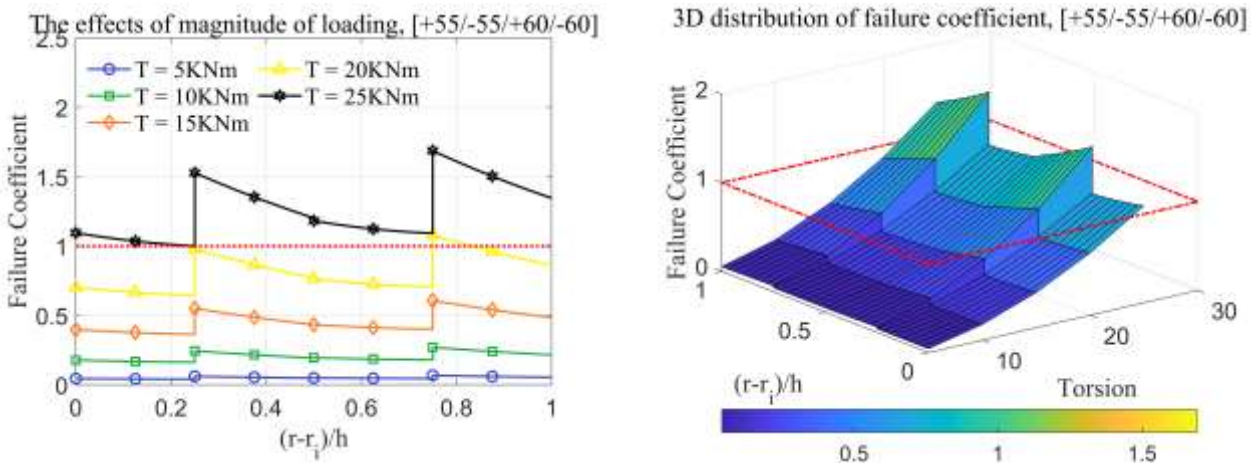

Figure 6. Effects of torsion magnitude on Modified Tsai-Hill failure coefficients across the normalized pipe thickness.

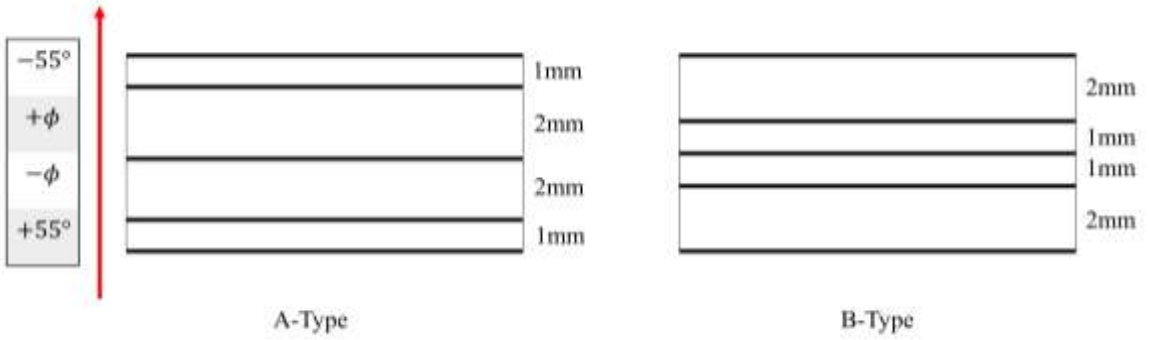

Figure 7. A-type and B-type pipes.

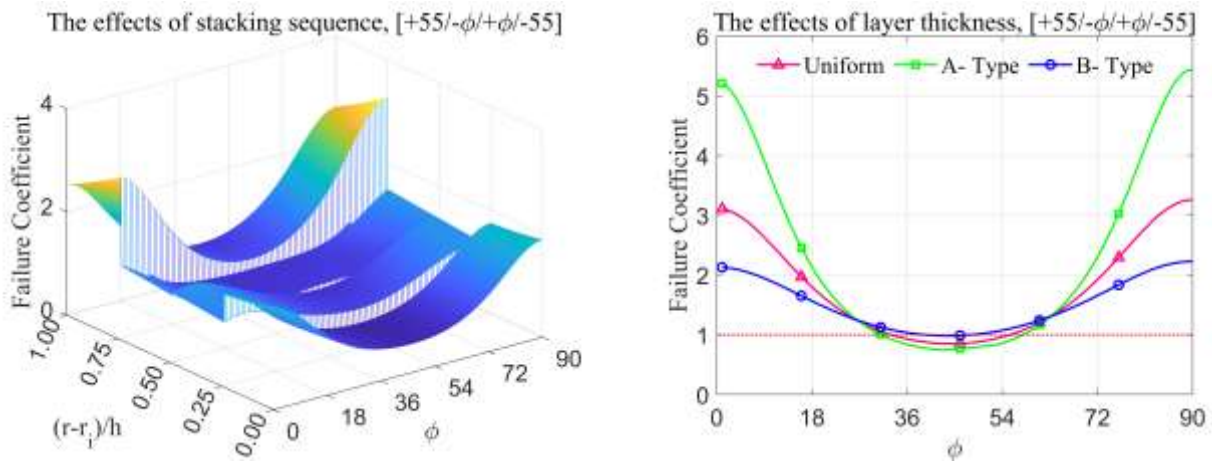

Figure 8. Effects of stacking sequence and layer thickness on failure coefficients distribution for pipe with $[+55°/-\phi°/+\phi°/-55°]$.

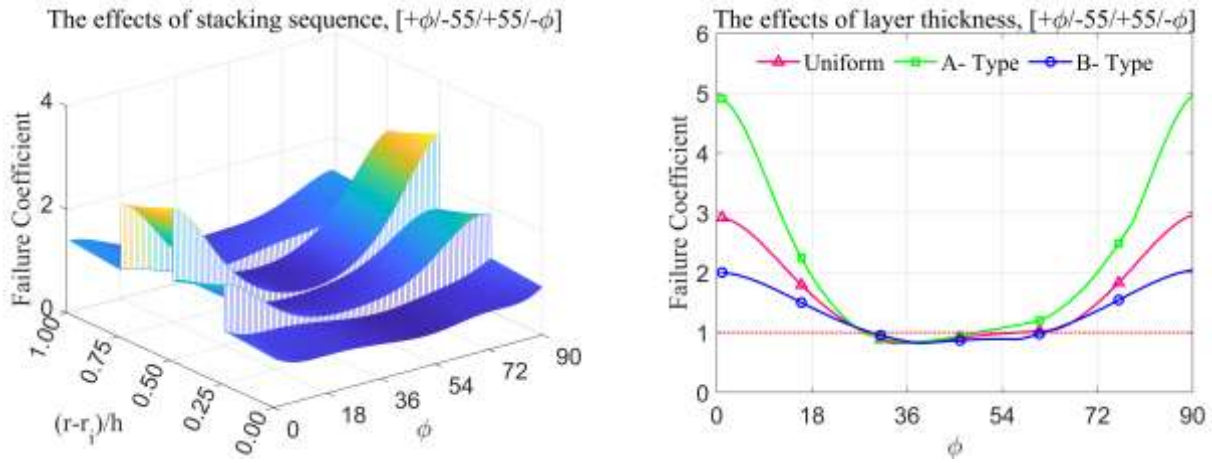

Figure 9. Effect of stacking sequence and layer thickness on failure coefficients distribution for pipe with $[+\phi°/-55°/+55°/-\phi°]$.

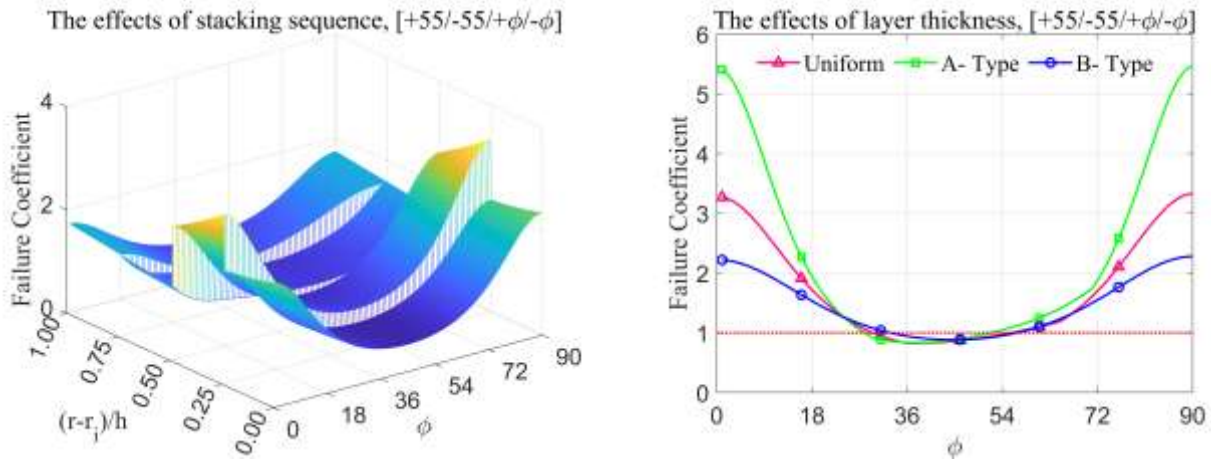

Figure 10. Effects of stacking sequence and layer thickness on failure coefficients distribution for pipe with $[+55°/-55°/+\phi°/-\phi°]$.

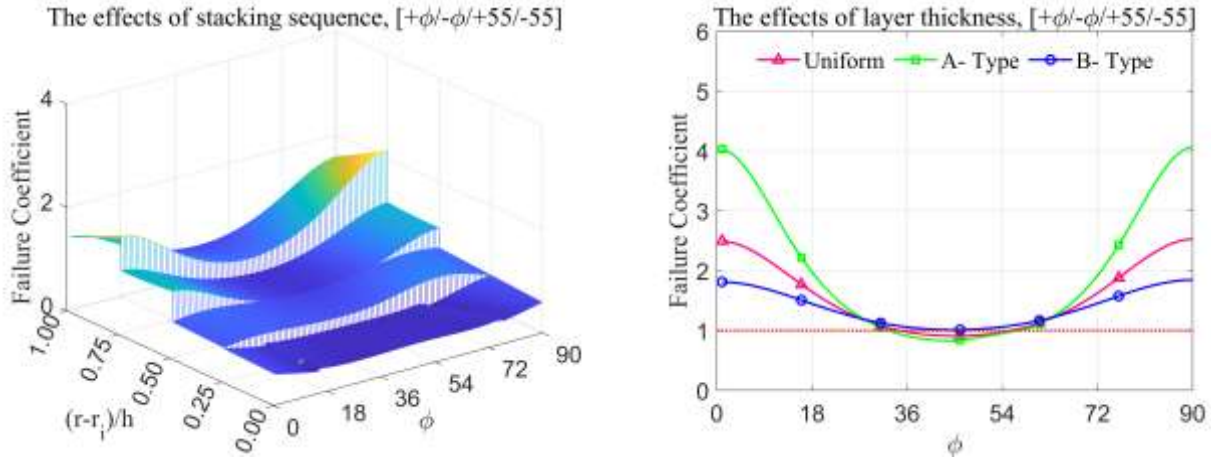

Figure 11. Effects of stacking sequence and layer thickness on failure coefficients distribution for pipe with $[+\phi°/-\phi°/+55°/-55°]$.

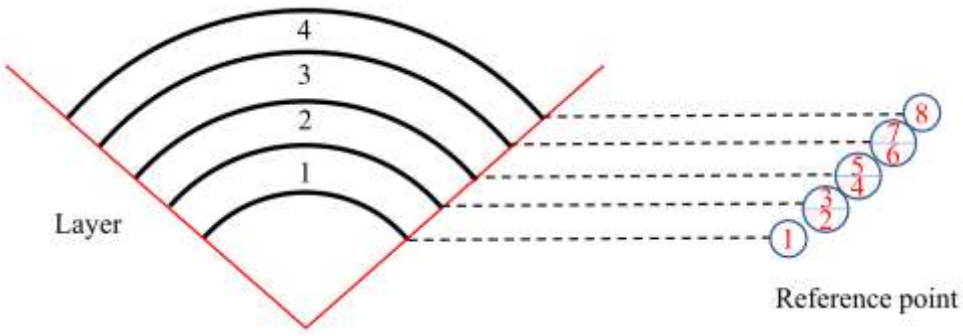

Figure 12. Reference points across the pipe thickness.

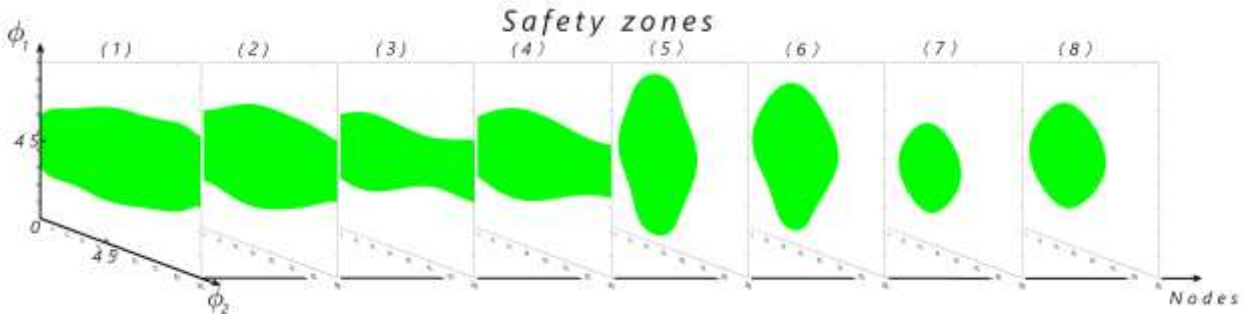

Figure 13. The safety zones at reference points.

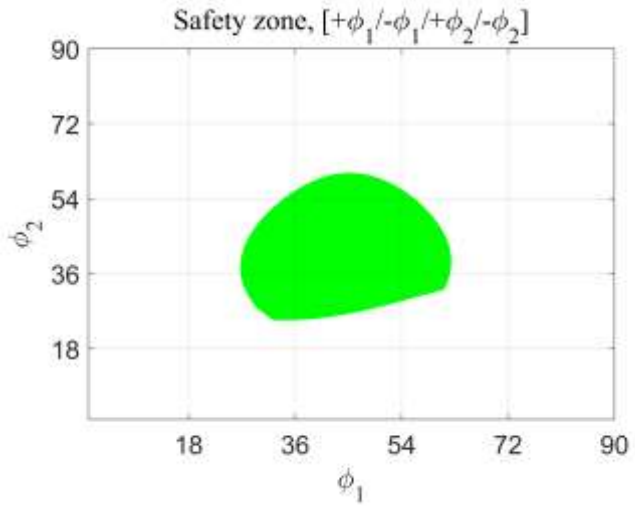

Figure 14. The allowable fibre angles for the pipe with $[+\phi_1/-\phi_1/+\phi_2/-\phi_2]$ lay-up.

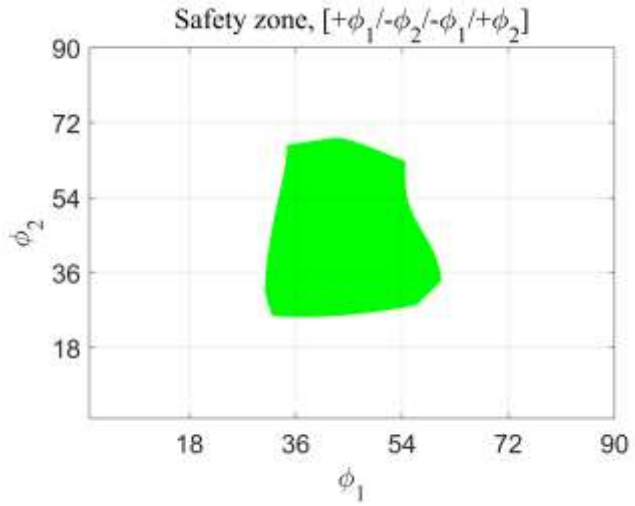

Figure 15. The allowable fibre angles for the pipe with $[+\phi_1/-\phi_2/-\phi_1/+\phi_2]$ lay-up.

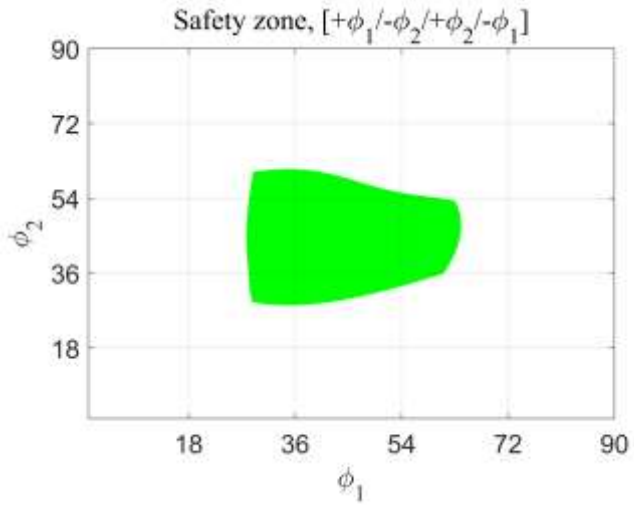

Figure 16. The allowable fibre angles for the pipe with $[+\phi_1/-\phi_2/+\phi_2/-\phi_1]$ lay-up.